THE JOURNAL OF PHYSICAL CHEMISTRY C

Article

pubs.acs.org/JPCC

Determination of the Optical Constants of Gold Nanoparticles from Thin-Film Spectra

Carlos Pecharroman,*[,†] Enrico Della Gaspera,[‡,§] Alessandro Martucci,[‡] Ramón Escobar-Galindod,[†,∥] and Paul Mulvaney[⊥]

[†]Instituto de Ciencia de Materiales de Madrid, CSIC, Madrid, Spain

[‡]Dipartimento di Ingegneria Industriale Via Marzolo 9, Universita' di Padova, 35131 Padova, Italy

[§]CSIRO Manufacturing, Bayview Avenue, Clayton, VIC 3168, Australia

[∥]Abengoa Research S.L., Abengoa, Campus Palmas Altas, Sevilla 41014, Spain

[⊥]School of Chemistry and Bio21 Institute, University of Melbourne, Parkville, VIC 3010, Australia

Supporting Information

ABSTRACT: We determine the optical properties of nanocomposites comprising gold nanoparticles embedded in a titania matrix using spectroscopic ellipsometry. We then apply the spectral representation formalism due to Bergman, to extract the dielectric function of the individual gold nanoparticles (NPs). We show that analytical forms of the spectral representation function can be generated, which enable local clustering and the width of the surface plasmon resonance to be accounted for. The model also explains anomalously high, near-infrared absorption by small metal particles, reported by Tanner. The procedure provides a method to determine the optical constants of a wide range of metallic and semiconducting nanoparticles from ellipsometric data.

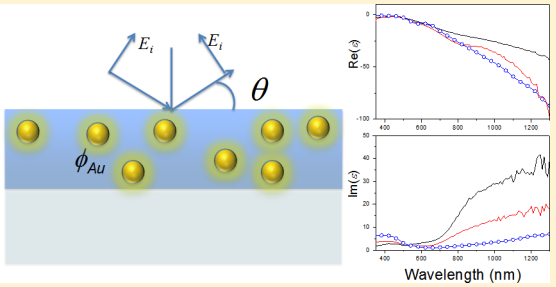

1. INTRODUCTION

Nanoparticles (NPs) have unique optical properties that can be exploited in a variety of applications ranging from optoelectronics to biolabeling, catalysis, and sensing. NPs can be dispersed into polymers, glasses, or gels to create macroscopic materials with unique optical properties. In the case of metal particles, such nanocomposites have attracted attention for over a century.[1−4] Dispersions of gold, silver, and copper NPs exhibit new optical resonances that are absent in bulk metal films. These unusual absorption features termed localized surface plasmon resonances (LSPRs) may be tuned by altering the shape and size of the metal particles, as well as their relative distance. LSPR bands have also been observed for NPs of reactive metals such as potassium, sodium, and lithium embedded in salt matrices.[5] More recently, attention has focused on semiconductor NPs, which exhibit strongly size-dependent, linear, and nonlinear optical spectra, once the crystallite size approaches the Bohr radius.[6] Schmitt-Rink and colleagues showed that composite films of such NPs may exhibit nonlinear resonances that can be tuned by the particle size.[7,8] For both metallic and semiconducting NPs, there is a need to be able to determine the frequency (ω) and size-dependent (R), dielectric function $\varepsilon(\omega,R)$ of the nanocrystal from experiment. In other words, given a nanocrystal-doped material, can one determine the dielectric properties of the embedded particles? Since one requires both the real and imaginary parts of the function over a reasonable wavelength regime, at least two independent optical measurements are needed at each wavelength. In the case of metal particles there have been two notable studies of this problem. In 1967, Fragstein and Schoenes measured both the absorption spectrum and the scattering spectrum from small gold particles.[9] Inversion of the Mie equations leads to two simultaneous equations for the dielectric function. In a more recent work, Poelsma et al. used ellipsometry to study the reflection coefficients of gold particles adsorbed as dense monolayers in air on a silica substrate.[10] However, while the dielectric function of the film was extracted, the authors did not attempt to determine the optical properties of the gold NPs themselves.

In order to understand the optical properties of highly dilute films of small spheres, one needs to take into account the polarization of the NP due to the effect of an external homogeneous field. In the case of single spheres of arbitrary size, the exact solution is given by the Mie equations.[2] However, in real systems, the particles are not isolated and inevitably present some level of aggregation or clustering, even for highly dilute systems. Moreover, it is often found that heterogeneous systems with identical composition present different effective properties due to variations in the spatial distribution of the components. Several models have been introduced to take this effect into account. The Maxwell−

Received: December 18, 2014
Revised: March 18, 2015
Published: April 6, 2015

DOI: 10.1021/jp512611m
J. Phys. Chem. C 2015, 119, 9450−9459

Garnett (MG) formalism[1] is most commonly used because of its simplicity and accuracy for dilute systems. However, the MG approximation assumes only dipolar interactions: therefore, when the particles approach one another this model becomes invalid. An improved approach is the effective medium theory (EMT), which gives more accurate results for moderately interacting systems.[11−13] The starting hypothesis of this formalism is that each particle is embedded in a homogeneous medium with the same dielectric constant as that of the composite. Both of these models assume spherical inclusions, although the MG theory has been extended to the case of small ellipsoids by Hayashi and Kanamori[14] and by Giordano.[15] A third approach is the spectral representation formalism, first formulated by Bergman.[16,17] This method assumes there is an exact solution to the problem of the effective dielectric constant of a composite once the so-called spectral representation function (SRF)[16] is known. This function, $g(n)$, which contains all the relevant geometric information about the composite, can be understood as a continuous distribution of the weights corresponding to all the possible depolarization factors of the particles (denoted n). Thus, the real problem is to determine this function. It is important to note that the problem of determining any electromagnetic property of one of the components (e.g., dielectric constant) from the corresponding effective value of the composite strongly depends on the quality of the experimental data. This is due to the mathematically ill-conditioned character of this problem. In such cases, even small errors, in either the experimental data or in the effective medium model can lead to large errors in the estimation of the effective property of the particles. Nevertheless, the SRF approach has been successfully applied by several groups to spherical metal nanocrystal composites. Felderhof and Jones have even incorporated higher-order multipole interactions into the SRF formalism,[18] while Pecharroman et al. have applied analytic forms of the SRF to the IR reflection of ionic crystals.[19]

In this work we introduce a phenomenological model for the SRF of diluted NPs. This approach has the advantage that it does not depend on the nature of the materials of the composite, and in the case of small metal particles, it predicts the resonance wavelengths and the strengths of the surface plasmon modes. These solutions are basically the spectral representation function of the system. As a consequence, we can account for clustering in dilute gold NP systems. The effective medium properties depend on both the nature of the components and the microstructure of the composite. Consequently, the determination of the optical properties of metallic NPs requires both a precise description of the composite microstructure, given by $g(n)$, and also accurate refractive index experimental data for the composite films. Knowing this, one can immediately determine the dielectric properties of the metallic NPs, their state of aggregation within the film, and their influence on the effective dielectric properties of the composite film.

Here, we present the procedure to determine the SRF parameters and demonstrate its applicability to the case of gold NPs dispersed in a thin metal oxide film. However, the methodology is general and can be applied to a wide range of composites comprising small particles such as magnetic or semiconducting nanocrystals embedded within a homogeneous matrix.

2. THEORETICAL MODEL

2.1. Determination of the Refractive Index of Thin Layers by Small Perturbation Ellipsometry. In spectroscopic ellipsometry, the reflection coefficients of a thin film coating an infinitely thick, nonabsorbing slab are determined as a function of wavelength for several angles of incidence. These procedures usually employ nonlinear, least-squares fitting methods to determine both the thickness and complex refractive index of the layer.[20] However, in the case of small changes in the film properties, such as those introduced by doping with NPs, it is possible to treat the complex reflectance ratio (ρ) as a small perturbation to the behavior of the system. The magnitude of this ratio can be obtained from the usual ellipsometric parameters, $\tan(\Psi)$ and $\cos(\Delta)$

$$\hat{\rho}(\theta, \lambda) = \tan(\Psi(\theta, \lambda))e^{i\Delta(\theta,\lambda)} \tag{1}$$

This explicit expression for the complex reflectance ratio depends primarily on the angle of incidence (θ) and on the wavelength (λ) but also on the nature and structure of the sample. However, all the samples considered in this work comprise transparent silica glass substrates coated with a single thin film of either titania or titania-containing Au NPs. For this particular configuration, the reader can find the explicit expressions for eq 1 in the Supporting Information, section 1.

If the complex reflectance ratio of the pure titania film is known, the incremental shift in the refractive index due to small modifications in thickness (δh) and refractive index (δm) of the layer can be written as a series expansion

$$\hat{\rho}(\theta, m, h) = \hat{\rho}_0(\theta, m_0, h_0) + \frac{\partial\hat{\rho}}{\partial h}\delta h + \frac{1}{2}\frac{\partial^2\hat{\rho}}{\partial h^2}\delta h^2 + \frac{\partial\hat{\rho}}{\partial m}\delta m \tag{2}$$

where θ is the angle of incidence, h the layer thickness, and m the refractive index. We have expanded the series up to δh^2 to allow for small thickness differences between the doped and undoped layers. In order to calculate ρ_0 and the derivatives of ρ, Fresnel coefficients can be used (numerically calculated as shown in the Supporting Information). Operating on eq 2 the increment in the refractive index is given by

$$\delta m = \frac{(\hat{\rho}(\theta, m, h) - \hat{\rho}_0(\theta, m_0, h_0)) - \left(\frac{\partial\hat{\rho}}{\partial h}\delta h + \frac{1}{2}\frac{\partial^2\hat{\rho}}{\partial h^2}\delta h^2\right)}{\frac{\partial\hat{\rho}}{\partial m}} \tag{3}$$

It should be noted that all the coefficients are complex numbers, and the increment in the refractive index refers to both the real and imaginary parts. The differences in the refractive indices are not very important, but as we will show later, in some spectral regions, small inaccuracies can have a very strong impact on the final results.

2.2. Determination of Dielectric Functions of Au NPs. Once the refractive index or the dielectric constant of a composite is known, the most difficult task is to deduce the optical properties of one of the components. In principle, it is necessary to know the constitutive law that relates the optical properties of the composite to the volume fractions and geometrical packing of each component. Here, the spectral representation formalism is the chosen method used to describe the constitutive behavior of the nanocomposite. According to the spectral representation formalism, the

DOI: 10.1021/jp512611m
J. Phys. Chem. C 2015, 119, 9450−9459

effective dielectric constant at a particular frequency or wavelength is given by[21]

$$\langle\zeta\rangle = f\int \frac{g(n)}{1/\zeta + n}\mathrm{d}n \tag{4}$$

where f is the filling factor; $\zeta = \varepsilon/\varepsilon_m - 1$, $\langle\zeta\rangle = \langle\varepsilon\rangle/\varepsilon_m - 1$; and ε, ε_m, and $\langle\varepsilon\rangle$ are the dielectric constants of the NPs, the matrix, and the composite, respectively. The spectral representation function, $g(n)$, can be considered to be the distribution function of the depolarization factors, n, present in the nanocomposite ($0 < n < 1$). Therefore, the SR formalism states that the effective dielectric constant is given by the Hilbert transform (eq 4) of $g(n)$. Using this formalism, the condition for excitation of a surface plasmon mode is

$$(1 - n_0)\varepsilon_m + n_0\varepsilon = 0 \tag{5}$$

where n_0 corresponds to the depolarizing factor for a single, isolated particle. It is well established that for dilute systems (<1 vol %) or for cases where the inclusions do not touch, the MG formalism gives accurate results. The MG approximation assumes that there are no particle interactions and that the inclusions are spheres. For the more general situation of arbitrary particle shape, governed by the single depolarization factor L ($L = 1/3$ for spherical inclusions), the MG model predicts

$$g_{\mathrm{MG}}(n) = \delta(n_0 - L(1 - f)) \tag{6}$$

where δ is the delta function. Conversely, when there are significant interactions between the particles, the SRF becomes a broad, continuous function.[21] In real plasmonic composites with metal concentrations less than 5 v/v%, both isolated particles and small clusters are found. Hence, neither the MG nor effective medium models give an accurate description of the composite material. Consequently, we have designed a specific SRF which will be valid for "dilute" systems. This regime includes composites with concentrations below the percolation threshold but with some kind of multipolar interparticle interaction due to clustering.

When the particles start to interact (weak coupling), the effective depolarization factor along the direction of the axis dimer shifts to lower values, while the perpendicular component remains largely unchanged. Furthermore, multipolar modes[22] or aggregation effects may appear as secondary modes.[23] These new features are strongly dependent on the interparticle separation. Because in a composite there is a continuous distribution of distances between the particles, the SRF of a random and dilute distribution of spheres should be a continuous superposition of delta functions, exhibiting a maximum slightly below the position of that corresponding to the single-particle depolarization factor.[22−24] It is precisely this particle coupling that is responsible for the broadening of the SRF. It is important to note that the particles do not need to be actually touching. Even in a dilute particle distribution, there will always be a small fraction of particles relatively close to each other.

Although the choice of SRF is arbitrary,[25] the selected function should have specific properties consistent with the type of system under study. For the present case we have chosen a Lorentzian profile for the SRF

$$g(n) = A\left(\frac{1}{(n - n_0)^2 + w^2} - \frac{1}{c^2 + w^2}\right) \tag{7}$$

Here n_0 is the average depolarization factor, and w is the Lorentzian width. This function is determined by the shape, and relative distances distribution of the particles within the composite. It has the important property that its Hilbert transform (eq 4) is an analytical function and hence is easy to evaluate. The function only takes positive values in the interval around n_0, defined by $n_0 - c < n < n_0 + c$. By limiting the SRF to these values, we ensure that there is no weighting given to percolated clusters, which appear at $n = 0$. This condition is satisfied when $c \leq n_0$. Finally, the normalization constant A is determined from the SRF sum rule, which for nonpercolated systems is given by

$$\int_{n_0-c}^{n_0+c} g(n)\mathrm{d}n = 1 \tag{8}$$

This yields

$$A = \frac{1}{2}\frac{w(c^2 + w^2)}{(c^2 + w^2)\arctan\left(\frac{c}{w}\right) - wc} \tag{9}$$

The dielectric constant can be analytically obtained by integrating eq 4 using eqs 8 and 9

$$\begin{aligned}\langle\zeta\rangle = f\Bigg[&\zeta(1 + n_0\zeta)(c^2 + w^2)\arctan\left(\frac{c}{w}\right)\\ &- \frac{w}{2}[1 + 2\zeta n_0 + (n_0^2 - c^2)\zeta^2]\ln\left(\frac{1 + \zeta(n_0 + c)}{1 + \zeta(n_0 - c)}\right)\Bigg]\\ /&\Bigg\{\left[(c^2 + w^2)\arctan\left(\frac{c}{w}\right) - cw\right][1 + 2\zeta n_0\\ &+ (n_0^2 + w^2)\zeta^2]\Bigg\}\end{aligned} \tag{10}$$

It should be noted that the c parameter can be chosen arbitrarily if the condition $c \leq n_0$ is satisfied. For the sake of convenience, we have fixed the value of c to $c = n_0/2$ so that eq 10 becomes

$$\begin{aligned}\langle\zeta\rangle = f\Bigg[&\zeta(1 + n_0\zeta)\left(\frac{n_0^2}{4} + w^2\right)\arctan\left(\frac{n_0}{2w}\right)\\ &- \frac{w}{2}\left[1 + 2\zeta n_0 + \frac{3}{4}n_0^2\zeta^2\right]\ln\left(\frac{2 + 3\zeta n_0}{2 + \zeta}\right)\Bigg]\\ /&\Bigg\{\left[\left(\frac{n_0^2}{4} + w^2\right)\arctan\left(\frac{n_0}{2w}\right) - \frac{n_0 w}{2}\right][1 + 2\zeta n_0\\ &+ (n_0^2 + w^2)\zeta^2]\Bigg\}\end{aligned} \tag{11}$$

For $w = 0$, eq 11 can be drastically simplified as follows

$$\langle\zeta\rangle|_{w\to 0} \to f\frac{\zeta}{1 + n_0\zeta} \tag{12}$$

$$\langle\varepsilon\rangle|_{w\to 0} \to \varepsilon_m\left(1 + f\frac{\varepsilon - \varepsilon_m}{\varepsilon_m(1 - n_0) + \varepsilon n_0}\right) \tag{13}$$

which is just the MG approximation ($\zeta = \varepsilon/\varepsilon_m - 1$, $\langle\zeta\rangle = \langle\varepsilon\rangle/\varepsilon_m - 1$ and $n_0 = L(1 - f)$).

DOI: 10.1021/jp512611m
J. Phys. Chem. C 2015, 119, 9450−9459

If the inclusions within the nanocomposites are well dispersed, the SRF generates small values for the w parameter. It is then interesting to go further than eq 11 and check how the MG approximation 12 is modified for nearly monodisperse systems (sharp but finite SRF). After a power series expansion of eq 11 in w, we find

$$\langle\zeta\rangle|_{w\to 0} = f\left[\frac{\zeta}{1+n_0\zeta}\left(1+\frac{4w}{\pi n_0}\right) + w\left(\frac{(2+n_0\zeta)(2+3n_0\zeta)}{n_0^2\pi(1+n_0\zeta)^2}\log\frac{2+n_0\zeta}{2+3n_0\zeta}\right)\right] \tag{14}$$

This equation tends to the MG approximation 12, for a very narrow SRF.

2.3. Relationship between the SPR and the SRF. Due to the very general assumptions involved in the derivation of eq 11, it should be able to describe the optical properties of moderately dilute nanocrystal ensembles. We now focus explicitly on the case of small gold NPs. In order to describe the optical response around the SPR, it is convenient to introduce the variable η, which can be considered to be an SPR detuning parameter

$$\zeta = -\frac{1}{n_0} + \eta \tag{15}$$

It should be noted that for $\eta = 0$ the SPR condition is fulfilled when eq 5 is satisfied. If we substitute eq 15 into eq 11 and expand this expression for low values of η and w, we obtain

$$\langle\zeta\rangle = -f\frac{\eta + i\frac{w}{n_0^2}}{n_0^2\eta^2 + \left(\frac{1}{n_0}-\eta\right)^2 w^2} \tag{16}$$

This is an interesting expression because it converts eq 11 into a relatively simple Lorentzian function. Additionally it should be noted that eq 16 does not depend on c, which is an arbitrary parameter. The explicit expression for $\langle\varepsilon\rangle$ from eq 16 is given by

$$\langle\varepsilon\rangle = \varepsilon_m\left[1 - f\frac{\varepsilon_m}{n_0}\frac{\left(1-n_0+i\frac{w}{n_0}\right)\varepsilon_m + n_0\varepsilon}{[(1-n_0)\varepsilon_m + n_0\varepsilon]^2 + (\varepsilon_m-\varepsilon)^2 w^2}\right] \tag{17}$$

Equation 17 is entirely general and provides a direct correlation between the volume fraction of NPs in a composite f, the material properties through ε, and the mean and variance in the depolarization factors (n_0 and w, respectively). This equation is valid for any nanocomposite for small to moderate filling fractions.

2.4. Lineshape of the SPR. For "plasmonic metals" (i.e., Au, Ag, Cu, etc.), eq 16 can be used instead of expression 11 to predict the line shape of the SPR. At this point, we can assume a Drude model for the dielectric constant of the metallic NPs: here ω_p and γ are the bulk plasma and damping frequencies respectively; λ_p and λ_g are their corresponding wavelengths; and ε_∞ is the dielectric constant above ω_p. Therefore, the detuning parameter, according to the Drude model, can be written as

$$\eta \cong \left(\frac{1}{n_0} + \frac{\varepsilon_\infty}{\varepsilon_m} - 1\right) - \frac{\lambda^2}{\varepsilon_m\lambda_p^2} + i\frac{\lambda^3}{\varepsilon_m\lambda_p^2\lambda_g} \tag{18}$$

In this case, the SPR condition is fulfilled when $\mathrm{Re}(\eta) = 0$.

$$\lambda_{SPR} = \lambda_p\sqrt{\varepsilon_\infty + \varepsilon_m\left(\frac{1}{n_0} - 1\right)} \tag{19}$$

For convenience, we introduce the term δ, defined as $\lambda = \lambda_{SPR}(1+\delta)$, which describes the degree of SPR wavelength detuning. In the case of wavelengths close to the SPR ($\delta \ll 1$) the dielectric constant detuning factor is linearly dependent on the wavelength

$$\eta \cong \Lambda(-2\delta + i\Gamma)$$
$$\Lambda = \frac{\lambda_{SPR}^2}{\varepsilon_m\lambda_p^2}$$
$$\Gamma = \frac{\lambda_{SPR}}{\lambda_g} \tag{20}$$

According to this last equation, the "true" SPR wavelength is never actually attained because, in a realistic system, η always includes an imaginary component. It is the imaginary term that is responsible for the finite width of the SPR. It is interesting to follow the behavior of eq 16 in the vicinity of the SPR. In the case that $w = 0$ (noninteracting particles or MG approximation) eq 16 can be written as

$$\langle\zeta\rangle = \frac{f(-2\delta + i\Gamma)}{n_0^2\Lambda(4\delta^2 + \Gamma^2)} \tag{21}$$

The absorption spectrum, which corresponds to the imaginary part of $\langle\zeta\rangle$, is a Lorentzian function, with a maximum located at $\delta = 0$ and a width (taken at the inflection point) of $d_{SPR} = \Gamma/2\sqrt{3}$. In the case considered here, where the particle interaction becomes relevant, it can be shown that the maximum of the imaginary part of $\langle\zeta\rangle$ does not shift, but its width is modified as follows

$$d_{SPR} = \frac{\Gamma}{2\sqrt{3}}\left(1 + \frac{w}{n_0^2\Lambda\Gamma}\right) \tag{22}$$

Finally, from the definition of δ, it can be estimated that the imaginary part of the effective dielectric constant follows a Lorentzian-like curve, with a width of

$$w_{SPR} = \frac{\lambda_{SPR}\Gamma}{2\sqrt{3}}\left(1 + \frac{w}{n_0^2\Lambda\Gamma}\right) = \frac{\lambda_{SPR}^2}{2\sqrt{3}\lambda_g}\left(1 + \frac{w}{n_0^2}\frac{\varepsilon_m\lambda_p^2\lambda_g}{\lambda_{SPR}^3}\right) \tag{23}$$

This is a very useful expression. It indicates that the width of the optical absorption spectrum around the SPR of a dispersion of metallic NPs exhibits a nearly Lorentzian profile, centered at λ_{SPR}, while the width depends only on two factors: Γ, which is a small parameter depending on the mean free path of the electrons inside the metallic NP, and w, which basically describes the multipolar particle interaction. In the case of low interaction values such that $w \ll n_0^2\Lambda\Gamma$, the width of the SPR absorbance spectrum depends only on the physical properties of the NPs (under which circumstances one obtains the MG model). Conversely once the SRF width exceeds this value, the SPR absorption band broadens noticeably, so that for closely

DOI: 10.1021/jp512611m
J. Phys. Chem. C 2015, 119, 9450−9459

packed aggregates this will be the dominant mechanism of peak broadening. It should be noted that this model also accounts for asymmetric peak broadening, which is impossible to explain with standard EMT models.

2.5. NIR Broadening. The present model explains not only the origin of the SPR broadening observed in real NP ensembles but also the unusually intense IR absorption tail in the ensemble spectra, which has been reported by several research groups.[26,27] To demonstrate this, it is necessary to consider the case when the nanocrystal inclusions have a very large dielectric constant ($\varepsilon \to \infty$). This is the case in the IR region for materials composed of metallic NPs dispersed in insulating (nonabsorbing) matrices. Expanding eq 14 when $\zeta \gg 1$ yields

$$\langle\zeta\rangle|_{\varepsilon\to\infty} = f\frac{n_0\left(\frac{n_0^2}{4}+w^2\right)\left(\frac{\pi}{2}-\frac{2w}{n_0}\right)-\frac{3w}{8}n_0^2\ln(3)}{\left[\left(\frac{n_0^2}{4}+w^2\right)\left(\frac{\pi}{2}-\frac{2w}{n_0}\right)-\frac{n_0 w}{2}\right](n_0^2+w^2)} \tag{24}$$

Analysis of eq 24 reveals that the effective dielectric properties of unpercolated heterogeneous systems are only a small perturbation to the corresponding values of the pure matrix, even if the isolated inclusions have very large dielectric functions. In the case of the infrared region, metal NPs satisfy this condition, according to the Drude model.[27] Therefore, by using eq 18 in eq 24 and expanding as a power series and assuming $\lambda/\lambda_p \gg 1$ and $\lambda/\lambda_g \ll 1$ we obtain

$$\langle\zeta\rangle_{\lambda\to\infty} = \frac{\langle\varepsilon\rangle|_{\lambda\to\infty}}{\varepsilon_m} - 1 = \frac{f}{n_0}\left[1 - \frac{\varepsilon_m\lambda_p^2}{n_0\lambda_g^2} + \frac{\omega(4-3\log 3)}{n_0\pi} + \frac{\varepsilon_m\lambda_p^2}{n_0\lambda^2} + i\frac{\varepsilon_m\lambda_p^2}{n_0\lambda\lambda_g}\right] \tag{25}$$

This latter expression indicates that for low frequencies the composites will exhibit a dielectric constant very similar to that of the matrix but slightly increased by a term which is proportional to the volume concentration of the inclusions. Equation 25 can be used to determine the SRF for drude NPs. In fact, if the real part of ($\langle\zeta\rangle$) is fitted against $1/\lambda^2$ in the IR range, we get the following linear regression (see Figure S2, Supporting Information)

$$\frac{\mathrm{Re}\langle\varepsilon\rangle|_{\lambda\to\infty}}{\varepsilon_m} - 1 = a - \frac{b}{\lambda^2} \tag{26}$$

the coefficients a and b introduce some constraints on the possible values for w and n_0.

$$a \simeq \frac{f}{n_0}\left[1 + \frac{w(4-3\log 3)}{n_0\pi}\right]$$
$$b \simeq f\frac{\varepsilon_m\lambda_p^2}{n_0^2} \tag{27}$$

If we have a reasonable estimate of λ_p (which is approximately λ_p = 131 nm for bulk gold) the SRF parameters are unequivocally defined. Equations 26 and 27 allow the SRF itself to be evaluated through an unambiguous determination of the values of the parameters n_0 and w. This fact is of crucial importance when attempting to obtain realistic values for the dielectric function of NPs from optical measurements on nanocomposites.

3. EXPERIMENTAL METHODS

3.1. Materials Synthesis. Au NPs of about 14 nm in diameter were synthesized with the Turkevich method by reducing $HAuCl_4$ in water with sodium citrate.[28] The Au colloids were subsequently capped with poly(*N*-vinylpyrrolidone) (PVP), purified, and eventually stored as concentrated ethanolic solutions, as described in detail elsewhere.[29] Au colloids are in the cubic crystalline phase (ICDD No. 040714), and the crystallite size is 5.2 ± 1.3 nm, considerably smaller than the actual NP size evaluated from TEM images (14.1 ± 0.9 nm), suggesting that Au NPs are polycrystalline (see Supporting Information). Anatase TiO_2 NPs were synthesized via acid-catalyzed sol−gel reaction as described previously[30] and stored in methanolic concentrated solutions. The solutions used for thin-film deposition were prepared by mixing the methanolic suspension of TiO_2 NPs with PVP-capped Au NPs in ethanol and spin coating the final solutions on either Si or SiO_2 substrates, as described in ref 29. Samples were then annealed at 300 or 400 °C for 1 h in air in a muffle furnace. The prepared samples are summarized in Table 1.

Table 1. Nanocomposite Thin Films Synthesized in the Present Study

name	composition	heat treatment
TiO_2 300	TiO_2	300 °C
TiO_2−Au 300	TiO_2-containing Au NPs	300 °C
TiO_2 400	TiO_2	400 °C
TiO_2−Au 400	TiO_2-containing Au NPs	400 °C

3.2. Characterization Techniques. Dry powder samples of the NP colloidal solutions were characterized by X-ray diffraction (XRD) by using a Philips PW1710 diffractometer. Optical absorption spectra of solutions and films were measured using a Jasco V-570 spectrophotometer. Transmission electron microscopy (TEM) measurements of the metal NPs deposited on a carbon-coated copper grid were taken with a Philips CM10 TEM. The surface morphology of the samples was investigated with an xT Nova NanoLab scanning electron microscope (SEM). Transmittance at normal incidence and ellipsometry quantities Ψ and Δ were measured using a J.A. Woollam V-VASE spectroscopic ellipsometer in vertical configuration, at two different angles of incidence (65°, 75°). Optical constants n and k and film thickness were evaluated from Ψ, Δ, and the transmittance data using the WVASE32 ellipsometry data analysis software by fitting to Cauchy dispersion equations, Gaussian, and Tauc−Lorentz oscillators in the nonabsorbing region, Au SPR peak regime, and at the UV absorption edge, respectively.

Rutherford backscattering spectroscopy (RBS) experiments to determine the metal volume fraction (f), density, and film thickness were carried out with the 5 MV HVEE Tandetron accelerator at the Centro de Micro-Análisis de Materiales of Universidad Autónoma de Madrid.[31] The RBS experiments were performed using 3.035 MeV He^+ ions to make use of the cross-section resonance $^{16}O(\alpha,\alpha)^{16}O$ at that particular energy and, therefore, to improve the sensitivity to oxygen. The data were acquired simultaneously with two silicon surface barrier detectors located at scattering angles of 170° with an energy resolution of 16 keV and an ion dose of 10 μC per detector.

DOI: 10.1021/jp512611m
J. Phys. Chem. C 2015, 119, 9450−9459

The chemical composition of the films has been extracted using the RBX software.[32] The determination of the gold volume fraction from the RBS data is presented in the Supporting Information.

4. RESULTS AND DISCUSSION

The characterization of the prepared TiO_2 and Au NPs is presented in Figure S3 of the Supporting Information. XRD confirms the presence of crystalline anatase NPs (Figure S3a, Supporting Information), while TEM reveals particles of about 4 nm in diameter (Figure S3c, Supporting Information). The optical absorption spectrum of the anatase colloidal suspensions in methanol (Figure S3e, Supporting Information) reveals the strong UV absorption onset related to TiO_2 band gap, while the solution remains totally transparent in the visible range, as a consequence of the good colloidal stability, necessary to obtain high quality thin films. Crystalline Au colloids of about 14 nm in diameter can be seen in Figures S3b and S3d (Supporting Information). Au colloidal solutions in ethanol exhibit a pronounced SPR peak centered at about 523 nm, consistent with the NP size and the refractive index of ethanol (Figure S3f, Supporting Information).[33]

Nanocomposite thin films are prepared from these colloidal suspensions as described in the Experimental section. A detailed optical and morphological characterization has been published recently.[29] The thermal treatment at 300 and 400 °C has been chosen in order to remove most organic compounds and solvents but avoid excessive particle growth and sintering. In fact, Scherrer analyses of the XRD patterns of the deposited films (not shown) confirms that the Au crystallite size is the same as that of the as-prepared colloids, while TiO_2 crystallite size is slightly bigger at 400 °C (about 6 nm) compared to that of the sample annealed at 300 °C (4.5 nm, fairly close to the value for the as-synthesized colloids) due to thermally driven crystal growth. The morphology of the samples has been investigated using SEM, and the results are presented in Figure S4 (Supporting Information): the nanocomposite films are homogeneous and smooth, even if a slightly rougher surface is observed in the samples annealed at 400 °C, due to the increased size of the anatase grains. Metal NPs can be seen as brighter spots in the SEM micrographs, due to their greater scattering contrast with respect to the oxide matrix: they are homogeneously dispersed on a micron scale, and there is an absence of major aggregation or segregation phenomena.

The optical absorption spectra of the prepared films are presented in Figure 1. Samples annealed at 400 °C—both with and without Au NPs—show a higher diffuse absorbance compared to films annealed at 300 °C, as a consequence of the greater reflection arising from the increased refractive index of the nanocomposite, due to the reduction in porosity occurring after higher-temperature annealing. Samples containing Au NPs exhibit a pronounced LSPR peak centered at 600−630 nm, much more red-shifted compared to the same particles dispersed in ethanol, due to the greater refractive index of the anatase matrix; for the same reason, the LSPR band in the nanocomposite annealed at 400 °C is centered at lower energies compared to the sample annealed at 300 °C.

The main goal of this work is to demonstrate that, by using an accurate model for the effective dielectric constant of a composite, it is possible to obtain the intrinsic optical properties of a nanocrystal, even when the dielectric properties of the matrix itself are not known precisely. By annealing the titania matrix at two temperatures, we create two composites

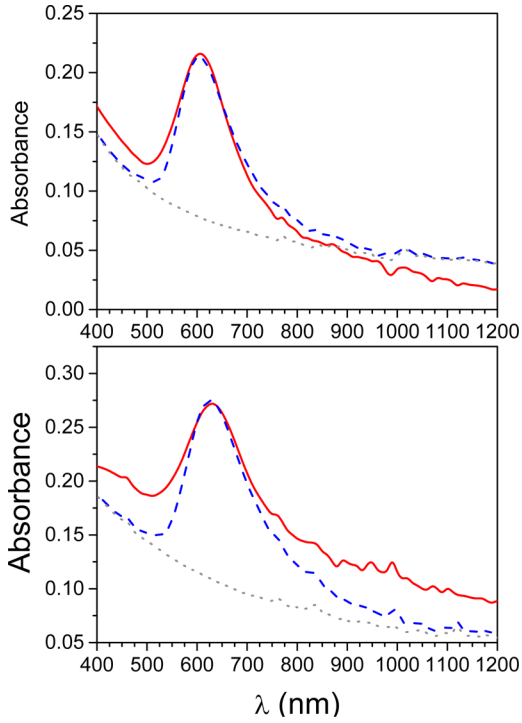

Figure 1. Absorption spectra of TiO_2 (dotted gray lines) and TiO_2−Au films annealed at 300 °C (top) and 400 °C (bottom). The continuous red lines are experimental spectra, and the dashed blue lines are calculated spectra using the gold dielectric constants determined from the ellipsometric data.

with different average refractive indices. However, if the theory outlined here is robust, we should extract the same dielectric properties for the embedded gold particles in each case. In order to obtain the dielectric constant of gold NPs it is absolutely necessary to have accurate values for the dielectric constant of the composite and undoped matrices (ε_m) and also for the gold volume concentration or filling factor (f). While ε_m can be determined by ellipsometric measurements on monolithic samples prepared in the same way as the composite films, the actual gold content in the annealed gold NP films is more difficult to measure, and therefore it was ultimately determined by RBS (see Figure S5, Supporting Information). The results of the film characterization are summarized in Table S1 (Supporting Information). The measured refractive indices of the titania nanoparticulate films were significantly less than that of bulk anatase due to the high film porosity.

Figure 2 shows the real and imaginary parts of the complex reflectance ratio of the titania films, with and without gold NPs. It is interesting to observe in these plots the aspect of the complex reflectance ratio for the TiO_2−Au composites. Both the real and imaginary parts look very similar to the expected increment of the dielectric constant in a composite, due to the inclusion of particles which present a SPR. After carrying out the manipulations, given by eq 3, and using the experimental film thicknesses determined by RBS, the complex refractive index curves corresponding to the TiO_2 and the TiO_2−Au film are obtained and are presented in Figure 3 along with the estimation using conventional ellipsometric software (Woollam).

There is no straightforward method to extract the dielectric constant of gold NPs from ellipsometric data. As we have mentioned before, most of inverse optical methods (i.e.,

DOI: 10.1021/jp512611m
J. Phys. Chem. C 2015, 119, 9450−9459

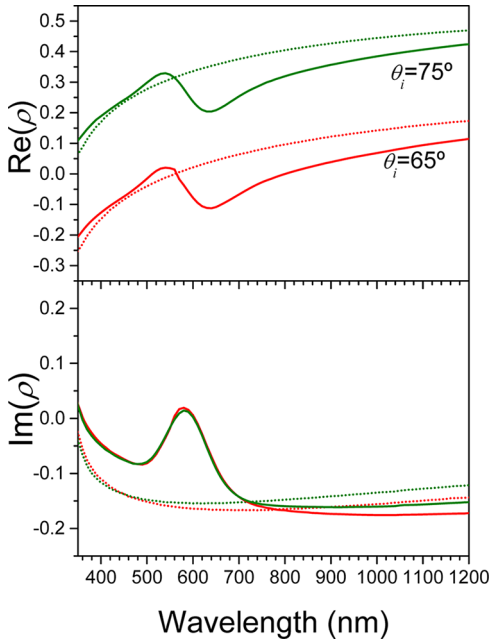

Figure 2. Experimentally obtained values of the complex function ρ collected at two angles of incidence (65°, red line; and 75°, green line) for TiO_2 (dotted lines) and TiO_2–Au films (continuous lines) annealed at 300 °C.

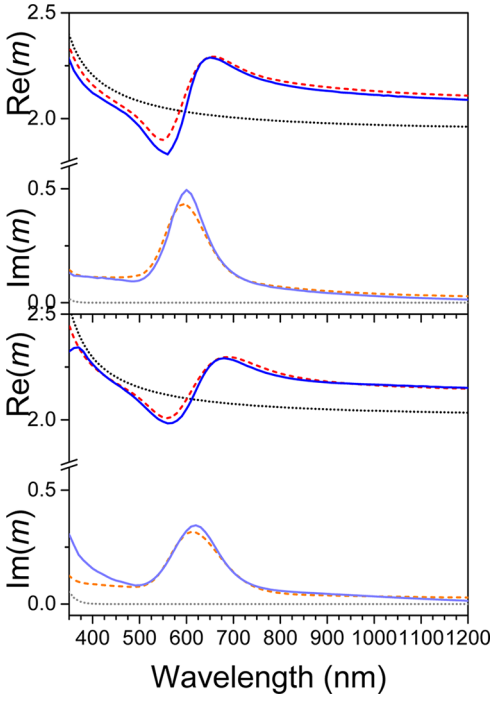

Figure 3. Real and imaginary parts of the refractive indices of TiO_2 and TiO_2–Au films annealed at 300 °C (upper graph) and at 400 °C (lower graph). The black dotted lines are the refractive indices of the TiO_2 film, while the red and blue lines are fits using the ellipsometer fitting software (Woolam) and from eq 3, respectively.

extraction of information from far-field scattering) are ill-conditioned problems, so that small errors in the measurements have a strong impact on the calculated results. To circumvent this limitation, high precision measurements as well as strong constriction on the fitting parameters are mandatory. To achieve this, we have collected high-quality ellipsometric optical data and made accurate determination of the key structural parameters of the composite (thickness, particle concentration, and degree of agglomeration). In the case of ellipsometric data, two sets of data corresponding to pure TiO_2 and composite TiO_2–Au layers on silica were required. By using the thickness data determined by RBS and ellipsometry, it has been possible to employ eq 3 to determine the change in refractive index as a consequence of the inclusion of gold nanocrystals. Once the refractive index (or dielectric constant) of the nanocomposites is known, the procedure to determine the refractive index of the NPs basically consists of inverting eq 4. However, this approximation requires a rough estimate of the value of the particle volume fraction and the SRF. We have found that most of the conventional methods to determine the particle concentration generated absolute errors of at least a few percent. Consequently, we employed RBS in order to minimize possible errors in this measurement.

From eq 9, the SRF function has a Lorentzian profile, so that it is completely determined by the distribution of depolarization factors (n_0) and the bandwidth (w). By carrying out a linear least-squares fit to the real part of the dielectric constant or $\mathrm{Re}(\langle\zeta\rangle)$ vs $1/\lambda^2$ in the IR region ($800 < \lambda < 1200$ nm), it is possible to determine the values of n_0 and w from eq 26. We found that $n_0 = 0.35$, $w = 0.091$ and $n_0 = 0.30$, $w = 0.11$ for the $T = 300$ °C and $T = 400$ °C samples, respectively. Finally, the complex value of ζ can be deduced from the experimental $\langle\zeta\rangle$ data (or ε from $\langle\varepsilon\rangle$) via numerical iteration at each wavelength. For this process, a MATLAB routine to minimize the following residual was employed[34]

$$\delta_l = |\langle\zeta\rangle_{\mathrm{exp},l} - \langle\zeta\rangle_{\mathrm{th}}(\hat{\varepsilon}_l, \hat{\varepsilon}_{m,l}, f, n_0, w, c)|;\ 0 \tag{28}$$

Here, $\langle\zeta\rangle_{\mathrm{exp}}$ refers to the optical measurement of the composite and $\langle\zeta\rangle_{\mathrm{th}}$ to the calculated values given by eq 11. It should be noted that δ_l (where l refers to each different measured wavelength) must satisfy the condition $\delta_l < 10^{-8}$ for every wavelength λ_l. In some spectral regions, it was impossible to obtain a valid solution to eq 11. These situations appear in the high-frequency domain ($\lambda < 400$ nm) where TiO_2 absorption dominates the spectrum and for wavelengths larger than 1200 nm, where the very high dielectric constant of the metal prevents convergence.

In Figure 4, we compare the extracted optical properties of the gold NPs with published bulk dielectric functions for gold.[35−37] While the results for the sample heated at $T = 400$ °C look very similar to those of bulk gold, at least over the spectral range $400 < \lambda < 1200$ nm, the sample treated at $T = 300$ °C yields a very different dielectric function. It is important to note that in eq 4 the integral variable n appears in the denominator along with $1/\zeta$. Therefore, only when the magnitude of $1/\zeta$ is comparable in size to n, which runs from 0 to 1, is the inversion process not ill-conditioned. This condition is satisfied for wavelengths around the SPR resonance, so that the procedure to determine the optical constants from composites exhibiting SPR phenomena is robust in this spectral region. For longer wavelengths, the high dielectric value of metal NPs, ε, forces the magnitude of $1/\zeta$ very close to zero, in such a manner that variations in ε do not produce a change in the effective value of eq 4. Additionally, there are strong discrepancies between the $T = 300$ and 400 °C samples, even in the SPR spectral region. In order to determine the nature of such differences, we have also included some modified dielectric functions in Figure 4, which incorporate

DOI: 10.1021/jp512611m
J. Phys. Chem. C 2015, 119, 9450−9459

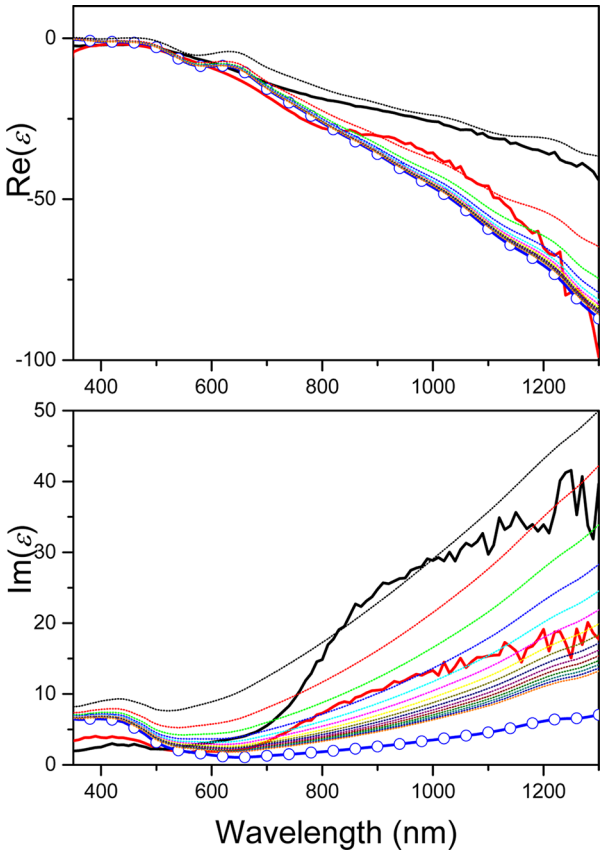

Figure 4. Complex dielectric function of the gold NPs extracted from the ellipsometric data using the SRF approach assuming $n_0 = 0.347$ and $w = 0.1$ (black lines: films annealed at 300 °C; red lines: films annealed at 400 °C) compared to the dielectric function of bulk gold[26] (blue line with circles). The dashed lines correspond to a series of modified dielectric functions of bulk gold (eq 29) for particle radii ranging from 1 to 15 nm in increments of 1 nm.

surface scattering effects,[35] calculated using the following expression

$$\gamma = \gamma_{\text{Bulk}} + 2\frac{Av_{\text{F}}}{D_{\text{eff}}} \tag{29}$$

Here $v_{\text{F}} = 1.4 \times 10^6$ m s^{-1} and $\gamma_{\text{Bulk}} \sim 1.64 \times 10^{14}$ s^{-1}[38] are the Fermi velocity and the damping equivalent wavelength for gold; D_{eff} is the effective particle size; and A is a phenomenological scattering parameter. We have used a value of $A = 1$. Equation 29 can be rewritten as

$$\frac{1}{\lambda_{\text{G}}} = \frac{1}{\lambda_{\text{G,Bulk}}} + \frac{1}{\lambda_{\text{G,Size}}}$$

$$\lambda_{\text{G,Size}} \simeq 850 D_{\text{eff}} \tag{29a}$$

It can be estimated that $\lambda_{\text{G,Bulk}} \sim 10^5$ nm, and consequently, the particle size will have an appreciable effect on the dielectric function of gold when $\lambda_{\text{G,Size}} < \lambda_{\text{G,Bulk}}$. This condition is met for $D_{\text{eff}} \sim 15$ nm. Therefore, in Figure 4, we have presented a series of modified dielectric functions, corresponding to particles with radii ranging from 1 to 15 nm. Our values of the imaginary part of the dielectric function are consistently higher than the values for bulk gold tabulated in the book edited by Palik.[35] For the sample heated at $T = 400$ °C there is reasonable agreement with modified dielectric functions corresponding to the actual particle size determined by the Debye–Scherrer method[29] ($r = 5$ nm). However, in the case of the sample heated at $T = 300$ °C, the effective particle size deduced from the surface electron scattering is much smaller ($D_{\text{eff}} \sim 1$ nm) than the physical particle size. This suggests the presence of crystalline defects. Equation 29 applies to any kind of defect which can perturb ballistic electron propagation. Gubicza et al.[39] have found that stacking faults are the most common defect in gold particles aged at room temperature. The presence of {111} facets is favored by their lower surface free energy. We also find that the particle sizes deduced from analysis of the (111) reflections by the Debye–Scherrer formula are generally larger than those determined from (h00) maxima. Analysis of the diffractograms from our composites also yields smaller crystallite sizes for (111) facets compared to (200) diffraction maxima (about a 50% decrease). Therefore, our ellipsometric data indicate that fresh gold nanoparticles consist of smaller crystallites, but once they are annealed above 300 °C, the crystals minimize their total energy by internal sintering processes to produce equiaxial crystalline domains.

Finally, it is useful to demonstrate how the methodology described here can be applied. The gold NPs were originally dispersed as a sol in ethanol. They were then dispersed into TiO_2 sol–gel matrices, and we have extracted their dielectric properties from these titania films. We now attempt to reproduce the original spectra in ethanol, which has a different dispersive refractive index.[40] The results are shown in Figure 5.

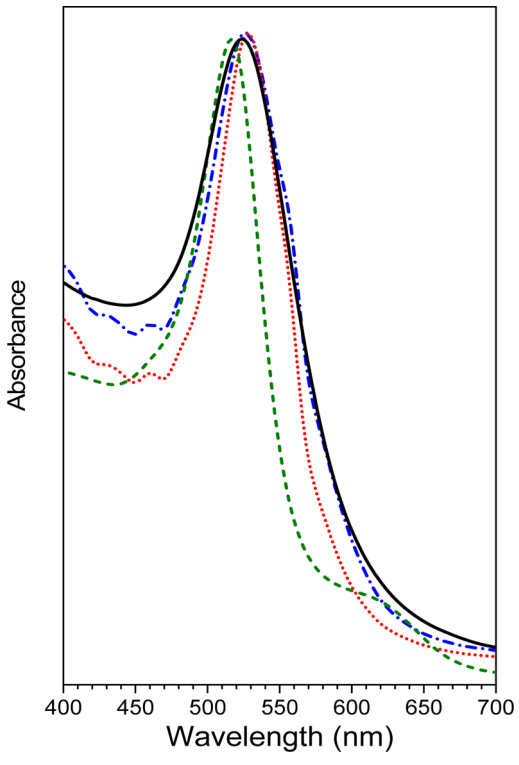

Figure 5. Experimental and calculated absorption spectra of a 15 nm gold colloid in ethanol. Black continuous line: experimental spectrum. Blue dashed-dotted line: calculated spectrum using a Lorentzian-shaped SRF and assuming $n_0 = 0.347$ and $w = 0.043$ derived from the analysis of the TiO_2/Au $T = 300$ °C composite. Red dotted line: calculated spectrum using the MG model with the same optical data. Green dashed line: calculated spectrum using a Lorentzian-shaped SRF with $n_0 = 0.347$ and $w = 0.043$ but employing bulk gold dielectric data.

DOI: 10.1021/jp512611m
J. Phys. Chem. C 2015, 119, 9450–9459

We have employed the optical parameters extracted from the TiO_2–Au nanocomposites that were annealed at the lowest temperature (T = 300 °C). It is evident that the SRF dielectric function determined from TiO_2–Au nanocomposites at T = 300 °C nearly exactly reproduces the absorption spectrum of the Au colloid in ethanol. Because the liquid medium contains the same gold particles but at a smaller concentration, we have used the same value of n_0 that was obtained from the solid composite but a lower value of w = 0.043 for the colloid, which is around half of the composite, w = 0.1. It is interesting to note that both surface scattering and SRF broadness cause an increase in the width of the SPR optical absorption peak. It is also clear from Figure 5 that the MG model, using the dielectric function corresponding to small nanoparticles, generates a peak whose fwhm is at least 20% smaller than that of the present model and fits the experimental spectrum poorly in comparison. We have also included a theoretical curve calculated using a Lorentzian-shaped SRF but employing the dielectric function of bulk gold.[35] This peak appears 9 nm blue-shifted, and its width is around half that calculated using the size-corrected dielectric function. Therefore, it can be concluded that when fitting the optical spectra both clustering and surface scattering need to be accounted for, and effective medium models are necessary.

5. CONCLUSIONS

We have presented a method for extracting the optical properties of NPs from moderately dilute homogeneous films of the NPs. We find that even in dilute samples local clustering of the particles leads to weak coupling of the polarization fields. For metal NPs, the clustering leads to broadening of the SPR. This phenomenon can be accounted for using the spectral representation function, which allows a distribution of depolarization factors to be included. A difficulty of the method is that clustering effects cannot be separated from shape heterogeneity effects. This is a common issue for reverse scattering methods. However, for chemically synthesized nanocrystal ensembles of well-defined morphology—for which the depolarization factor L (n_0) can be determined independently—the method allows the optical constants to be extracted directly from experimental optical measurements. The approach can be applied to any system of NPs dispersed within thin films.

■ ASSOCIATED CONTENT

Ⓢ Supporting Information

Additional details about sample characterization, experimental techniques, and mathematical derivation are provided. This material is available free of charge via the Internet at http://pubs.acs.org.

■ AUTHOR INFORMATION

Corresponding Author

*E-mail: cpg@icmm.csic.es.

Notes

The authors declare no competing financial interest.

■ ACKNOWLEDGMENTS

P.M. thanks the ARC for support under grant LF100100117 and C.P. acknowledges support under Spanish MINECO (MAT2011-29174-C02-01).

■ REFERENCES

(1) Garnett, J. C. M.; Garnett, J. C. M. Colours in Metal Glasses and in Metallic Films. *Proc. R. Soc. London* **1904**, *73*, 443–445.
(2) Mie, G. Beiträge Zur Optik Trüber Medien, Speziell Kolloidaler Metallösungen. *Ann. Phys.* **1908**, *25*, 377–445.
(3) Gans, R.; Happel, H. Zur Optik Kolloidaler Metallösungen. *Ann. Phys.* **1909**, *334*, 277–300.
(4) Bohren, C. F.; Huffman, D. R. *Absorption and Scattering of Light by Small Particles*; Wiley: New York, 2008.
(5) Hughes, A. E.; Jain, S. C. Metal Colloids in Ionic Crystals. *Adv. Phys.* **1979**, *28*, 717–828.
(6) Efros, A. L.; Efros, A. L. Band-to-Band Absorption of the Light in Semiconductor Sphera. *Fizika Tverdogo Tela* **1982**, *16*, 1209–1214.
(7) Schmitt-Rink, S.; Miller, D. A. B.; Chemla, D. S. Theory of the Linear and Nonlinear Optical Properties of Semiconductor Microcrystallites. *Phys. Rev. B* **1987**, *35*, 8113–8125.
(8) Kyprianidou-Leodidou, T.; Caseri, W.; Suter, U. W. Size Variation of Pbs Particles in High-Refractive-Index Nanocomposites. *J. Phys. Chem.* **1994**, *98*, 8992–8997.
(9) von Fragstein, C.; Schoenes, F. J. Absorptionskoeffizient Und Brechungsindex Feinster Goldkugeln Im Nahen Ultrarot. *Z. Phys.* **1967**, *198*, 477–493.
(10) Wormeester, H.; Kooij, E. S.; Poelsema, B. Unambiguous Optical Characterization of Nanocolloidal Gold Films. *Phys. Rev. B* **2003**, *68*, 085406.
(11) Bruggeman, D. A. G. Calculation of Various Physics Constants in Heterogenous Substances I Dielectricity Constants and Conductivity of Mixed Bodies from Isotropic Substances. *Ann. Phys.* **1935**, *24*, 636–664.
(12) Pecharroman, C.; Iglesias, J. Effective Dielectric Properties of Packed Mixtures of Insulator Particles. *Phys. Rev. B* **1994**, *49*, 7137.
(13) Landauer, R. Electrical Conductivity in Inhomogeneous Media. *AIP Conf. Proc.* **1978**, *40*, 2–45.
(14) Hayashi, S.; Kanamori, H. Infrared Study of Surface Phonon Modes in A-Fe 2 O 3 Microcrystals. *J. Phys. C: Solid State Phys.* **1980**, *13*, 1529.
(15) Giordano, S. Effective Medium Theory for Dispersions of Dielectric Ellipsoids. *J. Electrost.* **2003**, *58*, 59–76.
(16) Bergman, D. J. The Dielectric Constant of a Composite Material—a Problem in Classical Physics. *Phys. Rep.* **1978**, *43*, 377–407.
(17) Kantor, Y.; Bergman, D. J. The Optical Properties of Cermets from the Theory of Electrostatic Resonances. *J. Phys. C: Solid State Phys.* **1982**, *15*, 2033.
(18) Felderhof, B. U.; Jones, R. B. Effective Dielectric Constant of Dilute Suspensions of Spheres. *Phys. Rev. B* **1989**, *39*, 5669–5677.
(19) Pecharroman, C.; Gordillo-Vazquez, F. J. Expansion of the Spectral Representation Function of a Composite Material in a Basis of Legendre Polynomials: Experimental Determination and Analytic Approximations. *Phys. Rev. B* **2006**, *74*, 035120–1/10.
(20) Fujiwara, H. *Spectroscopic Ellipsometry: Principles and Applications*; Wiley: New York, 2007.
(21) Ghosh, K.; Fuchs, R. Spectral Theory for Two-Component Porous Media. *Phys. Rev. B* **1988**, *38*, 5222–5236.
(22) Pecharroman, C. Influence of the Close Sphere Interaction on the Surface Plasmon Resonance Absorption Peak. *Phys. Chem. Chem. Phys.* **2009**, *11*, 5922–5929.
(23) Ghosh, K.; Fuchs, R. Critical Behavior in the Dielectric Properties of Random Self-Similar Composites. *Phys. Rev. B* **1991**, *44*, 7330–7343.
(24) McPhedran, R. Asymptotic Studies of Closely Spaced, Highly Conducting Cylinders. *Proc. R. Soc.: Math., Phys. Eng. Sci.* **1988**, *415*, 185–196.
(25) Claro, F.; Fuchs, R. Optical Absorption by Clusters of Small Metallic Spheres. *Phys. Rev. B* **1986**, *33*, 7956–7960.
(26) Tanner, D. B.; Sievers, A. J.; Buhrman, R. A. Far-Infrared Absorption in Small Metallic Particles. *Phys. Rev. B* **1975**, *11*, 1330–1341.

DOI: 10.1021/jp512611m
J. Phys. Chem. C 2015, 119, 9450–9459

(27) Kim, Y. H.; Schmid, G. Possible Origin of the Anomalous Far-Infrared Absorption by Small Metal Particles. *Solid State Commun.* **2012**, *152*, 2129−2132.
(28) Enustun, B. V.; Turkevich, J. Coagulation of Colloidal Gold. *J. Am. Chem. Soc.* **1963**, *85*, 3317−3328.
(29) Della Gaspera, E.; Antonello, A.; Guglielmi, M.; Post, M. L.; Bello, V.; Mattei, G.; Romanato, F.; Martucci, A. Colloidal Approach to Au-Loaded Tio2 Thin Films with Optimized Optical Sensing Properties. *J. Mater. Chem.* **2011**, *21*, 4293−4300.
(30) Antonello, A.; Brusatin, G.; Guglielmi, M.; Bello, V.; Mattei, G.; Zacco, G.; Martucci, A. Nanocomposites of Titania and Hybrid Matrix with High Refractive Index. *J. Nanopart. Res.* **2011**, *13*, 1697−1708.
(31) Climent-Font, A.; Pászti, F.; García, G.; Fernández-Jiménez, M. T.; Agulló, F. First Measurements with the Madrid 5 Mv Tandem Accelerator. *Nucl. Instrum. Methods Phys. Res., Sect. B* **2004**, *219−220*, 400−404.
(32) Kótai, E. Computer Methods for Analysis and Simulation of Rbs and Erda Spectra. *Nucl. Instrum. Methods Phys. Res., Sect. B* **1994**, *85*, 588−596.
(33) Underwood, S.; Mulvaney, P. Effect of the Solution Refractive Index on the Color of Gold Colloids. *Langmuir* **1994**, *10*, 3427−3430.
(34) Optimization Toolbox, Matlab, The Mathworks Inc.,: Natick, MA, 2011.
(35) Lynch, D. W.; Hunter, W. R. Comments on the Optical Constants of Metals and an Introduction to the Data for Several Metals. In *Handbook of Optical Constants of Solids*; Palik, E. D., Ed.; Academic Press: Burlington, 1997; pp 275−367.
(36) Weaver, J. H.; Krafka, C.; Lynch, D. W.; Koch, E. E. *Appl. Optics* **1981**, *20*, 1124−1125.
(37) Kreibig, U. Kramers Kronig Analysis of the Optical Properties of Small Silver Particles. *Z. Phys.* **1970**, *234*, 307−318.
(38) Ung, T.; Liz-Marzán, L. M.; Mulvaney, P. Optical Properties of Thin Films of Au@Sio2 Particles. *J. Phys. Chem. B* **2001**, *105*, 3441−3452.
(39) Gubicza, J.; Lábár, J. L.; Quynh, L. M.; Nam, N. H.; Luong, N. H. Evolution of Size and Shape of Gold Nanoparticles During Long-Time Aging. *Mater. Chem. Phys.* **2013**, *138*, 449−453.
(40) Kedenburg, S.; Vieweg, M.; Gissibl, T.; Giessen, H. Linear Refractive Index and Absorption Measurements of Nonlinear Optical Liquids in the Visible and near-Infrared Spectral Region. *Opt. Mater. Express* **2012**, *2*, 1588−1611.

DOI: 10.1021/jp512611m
J. Phys. Chem. C 2015, 119, 9450−9459